SAR Change Imaging in the Sparse Transforming Domain Based on Compressed Sensing

Wenjiao Chen, Jiwen Geng, Ze Yu, *Member, IEEE*, and Yukun Guo

***Abstract*—Since compressed sensing (CS) theory broke through the limitation of the traditional Nyquist sampling theory, it has attracted extensive attention in the field of microwave imaging. However, conventional CS-based imaging models always suffer from the limitation of sparse properties of the scene itself. In this article, a novel change imaging in the transforming domain based on CS is proposed, which converts the recovery of the scene itself to that of scene change from the historical observation to the current observation. First, a new complex-data sparse microwave imaging model in the transforming domain is built by the real-imaginary separated operation. Then, a scene transform method named inverse-whitening processing is introduced to confirm the relationship between the real part, imaginary part, and amplitude part of a complex scene, and the sparse transforming domain is constructed based on this processing and historical observation. At last, a CS algorithm is used to recover this change with undersampling echo, and the scene of the current observation can be achieved by integrating the recovered change with the historical observation. The effectiveness of change imaging in the transforming domain is verified on both simulated and real synthetic aperture radar (SAR) images.**

***Index Terms*—Change imaging, compressed sensing (CS), inverse-whitening processing, synthetic aperture radar (SAR), transforming domain.**

I. Introduction

SYNTHETIC aperture radar (SAR) is a microwave remote sensing system that works in all-weather and all-day, and it plays an important role to observe key targets and hot regions [1]. In the traditional SAR system, the azimuthal resolution and range swath are irreconcilable contradictions for the limitation of the Nyquist sampling theorem. As the compressed sensing (CS) theorem is proposed [2], [3], [4], this contradiction can be effectively relieved and the nonlinear iteration algorithm can recover the sparse scene with sub-Nyquist samples. Some SAR systems based on CS have been proposed, e.g., AgileSAR [5], sub-Nyquist SAR [6], and CopSAR [7]. Compared with Sentinel-1, which can achieve 5 m resolution and 80 km swath [8], AgileSAR can achieve 5 m resolution and 300 km swath with a single azimuthal channel. Compared with the traditional high-resolution wide-swath (HRWS) SAR system, i.e., the azimuthal multichannel SAR [9] and multi-input multioutput SAR [10], the CS-SAR system has low system complexity, small antenna, and amount of data to relieve the pressure of data storage and transmission. Therefore, CS-SAR is an attractive and promising technology. However, these systems often require that the observed scene is sparse so the CS-SAR has a certain limitation. For example, CS algorithms only recover some significant features of the urban while other details are lost [5], [6], [7]. To further improve the universality and availability of sparse microwave imaging, we propose change imaging in the transform domain in the CS-SAR system.

For some scenes, which need frequent observation, the contents one acquired have changed a little with each other. In other words, the change denoted as $(\Delta\boldsymbol{\sigma})^{abs}$ is sparse, where $(\cdot)^{abs}$ denotes the amplitude of a complex signal. For these scenes, e.g., the urban area, CS algorithm can efficiently recover this sparse change instead of directly recovering the whole scene itself at each observation. Therefore, the concept of change imaging is proposed in this article. It means that the sparse change $(\Delta\boldsymbol{\sigma})^{abs}$ can be recovered by CS algorithms, and then the scene information $(\boldsymbol{\sigma}_1)^{abs}$ of the current observation can be achieved by integrating the recovered change $(\Delta\boldsymbol{\sigma})^{abs}$ with the historical observation $(\boldsymbol{\sigma}_0)^{abs}$. Obviously, the sparse property of scene change can guarantee the effectiveness of change imaging, and this property requires that the scene information of the current observation has consistency with that of the historical observation. This consistency includes temporal consistency and spatial consistency. Temporal consistency represents that the interval time between the historical observation and the current observation is not too long. For example, the change between Beijing's downtown in 2010 and that in 2022 is relatively big so change imaging may not be feasible. Spatial consistency guarantees the backscattering coefficient data of the observed scene does not change much. These factors that affect the radar cross section are usually represented by incidence angle, wavelength, and antenna polarization [11]. These factors also should not change much to ensure spatial consistency. Temporal consistency explains the property of changing parts of the observed scene, the latter corresponds to the property of the no-changing parts. Therefore, time consistency and spatial consistency guarantee the sparse property of scene change.

So far there are two similar works in sparse microwave radar imaging and they take good advantage of the CS theorem.

Manuscript received 31 July 2022; revised 16 September 2022; accepted 11 October 2022. Date of publication 21 October 2022; date of current version 10 November 2022. This work was supported by the National Natural Science Foundation of China under Grant 62271031. *(Corresponding author: Jiwen Geng.)*

Wenjiao Chen is with the School of Space Control and Communication, Space Engineering University, Beijing 102249, China (e-mail: chenwenjiao008@163.com).

Jiwen Geng is with the School of Information Science and Engineering, Southeast University, Nanjing 210096, China (e-mail: gengjiwen@buaa.edu.cn).

Ze Yu and Yukun Guo are with the School of Electronics and Information Engineering, Beihang University, Beijing 100191, China (e-mail: yz613@buaa.edu.cn; venik123@buaa.edu.cn).

Digital Object Identifier 10.1109/JSTARS.2022.3216322

Bi et al. [12] proposed a similar work, which applies change imaging in the SAR echo domain. However, the system requires that the satellite trajectories must be the same to obtain the echo change. This requirement is too strict to realize in the actual applications. The direct representation of scene change is the amplitude of the scene itself, so the simplest application of change imaging is also on the amplitude of the scene itself. To reduce the requirement for the observation geometry, Geng et al. [13] proposed an increment imaging in the SAR image domain. The increment imaging is essentially the same as change imaging, and it directly maps the amplitude of the scene itself. Because this method is an additively solving problem, i.e., $(\boldsymbol{\sigma}_1)^{abs} = (\boldsymbol{\sigma}_0)^{abs} + (\Delta\boldsymbol{\sigma})^{abs}$ and requires that the current observation $(\boldsymbol{\sigma}_1)^{abs}$ has the same quantification level with the historical observation, it is sensitive to the change's amplitude so that change imaging fails once the intermediate estimation goes wrong.

A good imaging algorithm should not have too many requirements for the system. To increase the universality and availability of sparse microwave imaging, we propose change imaging in the transform domain based on CS in this article. The idea of change imaging in the transform domain is that we transform the abovementioned additively solving problem into the multiplicatively solving problem, so we mainly pay attention to the signal form, not the absolute amplitude. At first, since the unrecovered current observation $\boldsymbol{\sigma}_1$ in the imaging is a complex signal and the recovered change $(\Delta\boldsymbol{\sigma})^{abs}$ is a real signal, we construct the complex-data optimization problem by real-imaginary separated operation. Then, a signal transform method we named inverse-whitening processing is introduced to confirm the relationship between the real part, imaginary part, and amplitude part of the scene change, and the sparse transforming domain is constructed based on inverse-whitening processing and the prior information of historical observation. At last, a CS algorithm is used to recover this change with undersampling echo, and the scene of the current observation can be achieved by integrating the recovered change with the historical observation. Simultaneously, adequate experimental results with the simulated signal and real SAR images demonstrate the effectiveness and universality of change imaging in the transforming domain. A summary of the main contributions of our work is listed as follows.

1) The idea of change imaging makes full advantage of the CS theorem, because scene change is easier to satisfy the sparse property compared with the scene itself. This imaging method can further decrease the sampling frequency and relieve the contradiction between high resolution and wide swath in the SAR system.
2) We apply change imaging in the transform domain and this method transforms an additively solving problem into a multiplicatively solving problem, so the estimation is not sensitive to the amplitude of the scene itself and improves imaging efficiency.
3) A complex-data optimization model in the change imaging is constructed by the real-imaginary separated operation. Simultaneously, a signal transform method named inverse-whitening processing is introduced to confirm the relationship between the real part, imaginary part, and amplitude part of the scene's change. A sparse transforming dictionary is constructed based on the historical observation data and the inverse-whitening processing.
4) Change imaging is applied to microwave sparse reconstruction, both simulation and experimental SAR data demonstrate the feasibility and effectiveness of our method in the transforming domain.

The rest of this article is organized as follows. In Section II, the change imaging signal model in the sparse transforming domain is introduced. In Section III, a signal transform method we named inverse-whitening processing is introduced, and then a sparse transforming dictionary is constructed based on this processing method and the historical observation. The current observation of the scene is achieved by integrating the historical observation with the recovered change based on the CS algorithm. In Section IV, numerical results demonstrate the effectiveness of our method. Finally, Section V concludes this article.

II. Changing Imaging Signal Model in the Sparse Transforming Domain

In this section, a sparse microwave imaging signal model is introduced. Usually, the SAR system is deemed to be stationary after transmitting one pulse and receiving one echo before the next transmitting [1], [11]. The raw data in the SAR system can be written as

$$\begin{aligned} s_c(\tau,\eta) = & \sum_{x_m,y_m} \sigma_m W_m(\tau,\eta) \\ & \exp\left\{ j\pi K_r [\tau - 2R_m(\eta)/c]^2 \right\} \\ & \cdot \exp\left(-j4\pi R_m(\eta)/\lambda\right) + n(\tau,\eta) \end{aligned} \tag{1}$$

where η and τ is the slow time along the azimuth and the fast time along the range, respectively. $R_m(\eta)$ represents the range between the radar and the point target located at the coordinate $(x_m, y_m, 0)$ at the azimuth time η. x_m and y_m denote the azimuth and range coordinates, respectively. Because two-dimensional image, i.e., azimuth and range, is considered, the coordinate $(x_m, y_m, 0)$ is simplified as (x_m, y_m). σ_m and $W_m(\tau,\eta)$ are the radar cross-section and the weighting pattern corresponding to the target at (x_m, y_m). K_r denotes the chirp rate of linear frequency modulated signal, c is the light speed, λ is the wavelength, and $n(\tau,\eta)$ is the system noise.

To relieve the inherent contradiction in the HRWS system, sub-Nyquist sampling in the CS-SAR system is implied along the azimuthal dimension. The CS-SAR system only adopts the traditional matched filtering (MF) method to not recover the scene exactly. Accordingly, CS-SAR imaging includes three steps: 1) range compression based on MF; 2) range cell migration correction (RCMC): interpolating by zero-padding every azimuthal signal after range compression, and then sum up all the range-compressed signals of grids on the same range cell to the predefined grid; 3) azimuth reconstruction with sub-Nyquist samples based on the CS algorithm. After implementing range compression and RCMC to the formula (1), the signal at a certain

range cell is represented by

$$s_c(\tau_0,\eta) = \sum_{x_m,y_m} \sigma_m W_m(\tau_0,\eta) T_r \sin c\left\{K_r T_r\left(\tau_0 - 2R_m(\eta-\eta_{cm})/c\right)\right\} \times \exp\left\{-j4\pi R_m(\eta-\eta_{cm})/\lambda\right\} + n(\tau_0,\eta) \quad (2)$$

where η_{cm} is the beam center crossing time for the target (x_m, y_m). T_r is the pulse width and sinc$(\cdot)$ denotes the *sinc* function.

Let $\boldsymbol{\sigma} = [\sigma_1, \sigma_2, \ldots, \sigma_M]^T$be the vectored backscattering cross-sections of targets on the same range cell, and $\mathbf{y}_{N\times 1} = [s_c(\tau_0,\eta_1), s_c(\tau_0,\eta_2), \ldots, s_c(\tau_0,\eta_N)]^T$ be the vectored signal after range compression and RCMC. The vectored signal can be modeled as

$$\mathbf{y}_{N\times 1} = \mathbf{A}_{N\times M}\boldsymbol{\sigma}_{M\times 1} + \mathbf{n}_{N\times 1} \quad (3)$$

where N is the sampling number on the azimuthal dimension, and M is the number of resolution cells at the certain range cell in the observed scene. $\mathbf{A}_{N\times M} = \{\mathbf{A}_m(\tau_0,\eta_n)\}_{n=1,m=1}^{N,M}$ denotes the mapping relationship between the received signal and the scene, and $\mathbf{A}_m(\tau_0,\eta_n) = W_m(\tau_0,\eta_n)\cdot T_r \cdot \exp\{-j4\pi R_m(\eta_n-\eta_{cm})/\lambda\}$. The noise is $\mathbf{n}_{N\times 1} = [n(\tau_0,\eta_1), n(\tau_0,\eta_2), \ldots, n(\tau_0,\eta_N)]^T$.

The CS theorem requires that the variable to be estimated is sparsely distributed. Nonlinear iterative algorithms can be implemented to recover the sparse scene, e.g., ship detection, by formula (3). However, many observed scenes do not have the sparse property so the development of the CS-SAR system is limited. Considering that some scenes themselves are not sparse but have a little change $(\Delta\boldsymbol{\sigma})^{abs}$ during each observation, change imaging is introduced by recovering the change $(\Delta\boldsymbol{\sigma})^{abs}$ and further recovering the whole scene by integrating the prior information of historical observation $(\boldsymbol{\sigma}_0)^{abs}$. And the current observation $(\boldsymbol{\sigma}_1)^{abs}$ is required to be consistent with the historical observation $(\boldsymbol{\sigma}_0)^{abs}$ so that it ensures the sparse property of change $(\Delta\boldsymbol{\sigma})^{abs}$. This consistency has temporal consistency and spatial consistency. Temporal consistency denotes that the current observation has similarities with historical observation and the interval time is not too long, so the change is small. For example, some areas may only add several targets in several days, the change is several targets and efficiently recovered by CS algorithms. Spatial consistency explains the consistency of backscattering coefficient data in the nonchange part of the scene. Because the observed incidence angle, wavelength, and antenna polarization affect the backscattering cross section [11], the consistency of the invariant part should be ensured. Temporal consistency and spatial consistency explain the property of the change part and invariant part, respectively. When this consistency is satisfied, we can apply change imaging in sparse microwave imaging to improve the universality of the CS-SAR system.

The simple and direct method of change imaging is applied in the spatial domain [13]. This method converts change imaging problem into additively solving problem, i.e., $(\boldsymbol{\sigma}_1)^{abs} = (\boldsymbol{\sigma}_0)^{abs} + (\Delta\boldsymbol{\sigma})^{abs}$. Only when the change $(\Delta\boldsymbol{\sigma})^{abs}$ has the same quantification level as the historical observation $(\boldsymbol{\sigma}_0)^{abs}$, the current observation $(\boldsymbol{\sigma}_1)^{abs}$ can be exactly recovered. Once $(\Delta\boldsymbol{\sigma})^{abs}$ is not exactly estimated or does not have the same quantification level, the change imaging fails. So the requirement in the spatial domain is strict. To improve the accuracy of the imaging algorithm, change imaging in the sparse transforming domain is proposed

$$\mathbf{y}_{N\times 1} = \mathbf{A}_{N\times M}\mathbf{D}_{M\times M}\Delta\boldsymbol{\sigma}_{M\times 1} + \mathbf{n}_{N\times 1}. \quad (4)$$

This method converts the imaging problem into a multiplicatively solving problem and is not sensitive to the scene amplitude itself.

III. Change Imaging in the Sparse Transforming Domain

In the abovementioned section, the change $(\Delta\boldsymbol{\sigma})^{abs}$ is explained to be sparse in the transforming domain, and it is a real signal. But the formula (4) in the sparse microwave imaging problem is the recovery of complex signals. Therefore, the following data structure for echo $\mathbf{y}$ and scene $\boldsymbol{\sigma}$ is established by the conversion from a complex signal to a real signal based on the real-imaginary separated operation. The real and imaginary parts of original complex data (3) and (4) are separated and can be expressed as

$$\begin{bmatrix} \mathbf{y}^{\text{real}} \\ \mathbf{y}^{imag} \end{bmatrix} = \begin{bmatrix} \mathbf{A}^{\text{real}} & -\mathbf{A}^{imag} \\ \mathbf{A}^{imag} & \mathbf{A}^{\text{real}} \end{bmatrix} \begin{bmatrix} \boldsymbol{\sigma}^{\text{real}} \\ \boldsymbol{\sigma}^{imag} \end{bmatrix} + \begin{bmatrix} \mathbf{n}^{\text{real}} \\ \mathbf{n}^{imag} \end{bmatrix} \quad (5)$$

$$\begin{bmatrix} \mathbf{y}^{\text{real}} \\ \mathbf{y}^{imag} \end{bmatrix} = \begin{bmatrix} \mathbf{A}^{\text{real}} & -\mathbf{A}^{imag} \\ \mathbf{A}^{imag} & \mathbf{A}^{\text{real}} \end{bmatrix} \begin{bmatrix} \mathbf{D}^{\text{real}}\Delta\boldsymbol{\sigma}^{\text{real}} \\ \mathbf{D}^{imag}\Delta\boldsymbol{\sigma}^{imag} \end{bmatrix} + \begin{bmatrix} \mathbf{n}^{\text{real}} \\ \mathbf{n}^{imag} \end{bmatrix}. \quad (6)$$

The sparse variable in the transforming domain is the amplitude part $(\Delta\boldsymbol{\sigma})^{abs}$, not the real part $(\Delta\boldsymbol{\sigma})^{\text{real}}$ or the imaginary part $(\Delta\boldsymbol{\sigma})^{imag}$. To achieve change imaging in the transforming domain, first, the relationship between the real part, imaginary part, and amplitude part of the scene should be analyzed and inverse-whitening processing is introduced to confirm this relationship. And then, the transforming dictionary $\mathbf{D}$ is constructed based on this processing method and the historical observation. At last, the underdetermined problem is recovered by CS algorithms.

A. Inverse-Whitening Processing

The phase distribution of SAR image follows an uniform distribution, real and imaginary parts of SAR image are similar to amplitude part [14], and it can also be demonstrated in Fig. 1. If the relationship between the real part, imaginary part, and amplitude part is certain, the real and imaginary parts can also be sparse in the transforming domain.

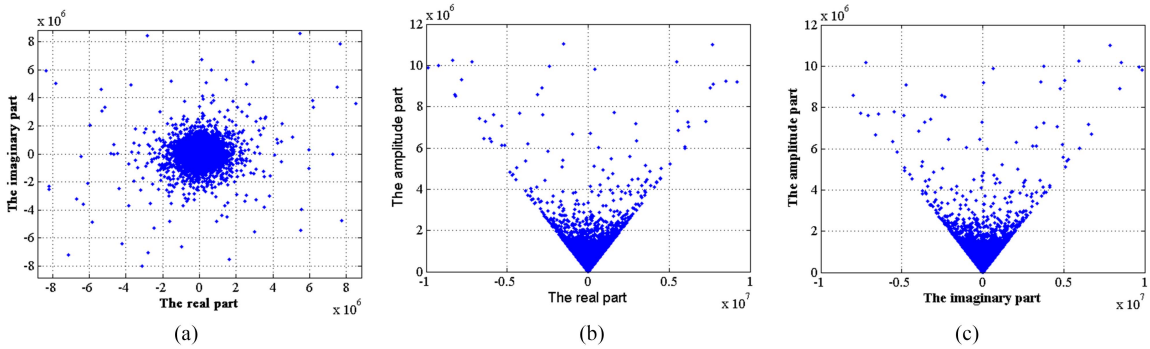

Fig. 1. Relationship between the real part, imaginary part, and amplitude part of the SAR image. (a) Relationship between the real part and imaginary part of the SAR image. (b) Relationship between the real part and amplitude part of the SAR image. (c) Relationship between the imaginary part and amplitude part of the SAR image.

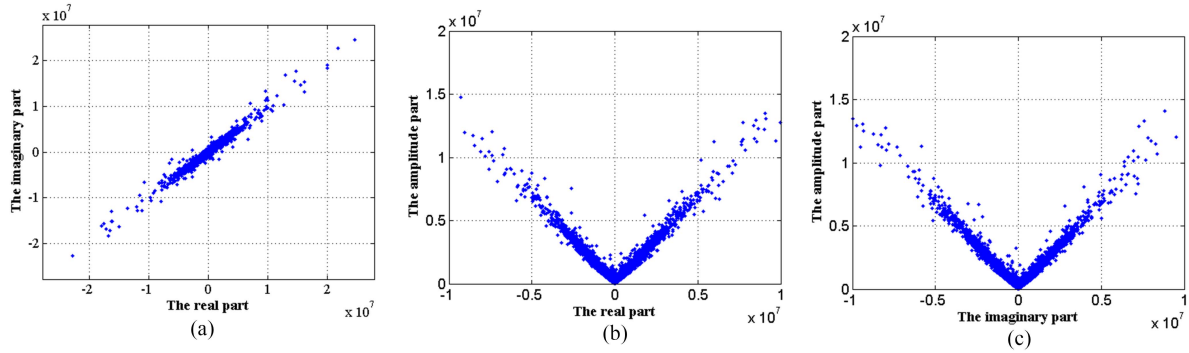

Fig. 2. Relationship between the real part, imaginary part, and amplitude part of the SAR image after inverse-whitening processing. (a) Relationship between the real part and imaginary part of the SAR image after inverse-whitening processing. (b) Relationship between the real part and amplitude part of the SAR image after inverse-whitening processing. (c) Relationship between the imaginary part and amplitude part of the SAR image after inverse-whitening processing.

In this article, a scene transform method named the inverse-whitening processing method is introduced by the scaling operation

$$\begin{bmatrix} (\boldsymbol{\sigma})_{\text{new}}^{\text{real}} \\ (\boldsymbol{\sigma})_{\text{new}}^{imag} \end{bmatrix} = \mathbf{Q} \cdot \begin{bmatrix} (\boldsymbol{\sigma})^{\text{real}} \\ (\boldsymbol{\sigma})^{imag} \end{bmatrix}$$

$$\mathbf{Q} = \begin{bmatrix} \cos\theta & -\sin\theta \\ \sin\theta & \cos\theta \end{bmatrix} \begin{bmatrix} a & 0 \\ 0 & b \end{bmatrix} \begin{bmatrix} \cos\theta & \sin\theta \\ -\sin\theta & \cos\theta \end{bmatrix} \tag{7}$$

$$\begin{aligned} (\boldsymbol{\sigma})_{\text{new}}^{\text{real}} &= \left(a\cos^2\theta + b\sin^2\theta\right)(\boldsymbol{\sigma})^{\text{real}} \\ &\quad + (a\sin\theta\cos\theta - b\sin\theta\cos\theta)(\boldsymbol{\sigma})^{imag} \\ (\boldsymbol{\sigma})_{\text{new}}^{imag} &= (a\sin\theta\cos\theta - b\sin\theta\cos\theta)(\boldsymbol{\sigma})^{\text{real}} \\ &\quad + \left(a\sin^2\theta + b\cos^2\theta\right)(\boldsymbol{\sigma})^{imag} \end{aligned}$$

to make the real part of the SAR image equal to the imaginary part of that

$$\left|(\boldsymbol{\sigma})_{\text{new}}^{\text{real}}\right| \approx \left|(\boldsymbol{\sigma})_{\text{new}}^{imag}\right| \approx (\boldsymbol{\sigma})_{\text{new}}^{abs} \Big/ \sqrt{2} \tag{8}$$

where $\mathbf{Q}$ is the scaling matrix, a and b are the scaling factors. θ is the rotating angle and is usually selected as $\pi/4$. This processing method is similar with the inverse operation of the whitening processing in traditional signal processing [15], so we name it inverse-whitening in this article. To acquire the formula (8), $(a-b)$ should be approximate to $(a+b)$. Additionally, to prevent the scaling matrix $\mathbf{Q}$ from being singular, a/b should not be too large. Assuming that $a/b = 10$, $\theta = \pi/4$, the data in Fig. 1 after inverse-whitening processing is illustrated in Fig. 2. In addition, Fig. 3 demonstrates that this scaling operation does not change the scene structure and just makes some adjustments to the scene amplitude. After inverse-whitening processing, the dynamic range of the SAR image in the probability histogram increases so that the image looks dim.

Now, the inverse-whitening processing is introduced to the observation model in (5)

$$\begin{aligned} &\begin{bmatrix} \mathbf{y}^{\text{real}} \\ \mathbf{y}^{imag} \end{bmatrix} \\ &= \begin{bmatrix} p_{11}\mathbf{A}^{\text{real}} - p_{21}\mathbf{A}^{imag} & p_{12}\mathbf{A}^{\text{real}} - p_{22}\mathbf{A}^{imag} \\ p_{11}\mathbf{A}^{imag} + p_{21}\mathbf{A}^{\text{real}} & p_{12}\mathbf{A}^{imag} + p_{22}\mathbf{A}^{\text{real}} \end{bmatrix} \\ &\quad \begin{bmatrix} \boldsymbol{\sigma}_{\text{new}}^{\text{real}} \\ \boldsymbol{\sigma}_{\text{new}}^{imag} \end{bmatrix} + \begin{bmatrix} \mathbf{n}^{\text{real}} \\ \mathbf{n}^{imag} \end{bmatrix} \end{aligned} \tag{9}$$

where the matrix $\mathbf{P} = \begin{bmatrix} p_{11} & p_{12} \\ p_{21} & p_{22} \end{bmatrix} = \mathbf{Q}^{-1}$, and $p_{11} = a^{-1}\cos^2\theta + b^{-1}\sin^2\theta$, $p_{12} = p_{21} = \left(a^{-1} - b^{-1}\right)\sin\theta\cos\theta$, $p_{22} = a^{-1}\sin^2\theta + b^{-1}\cos^2\theta$.

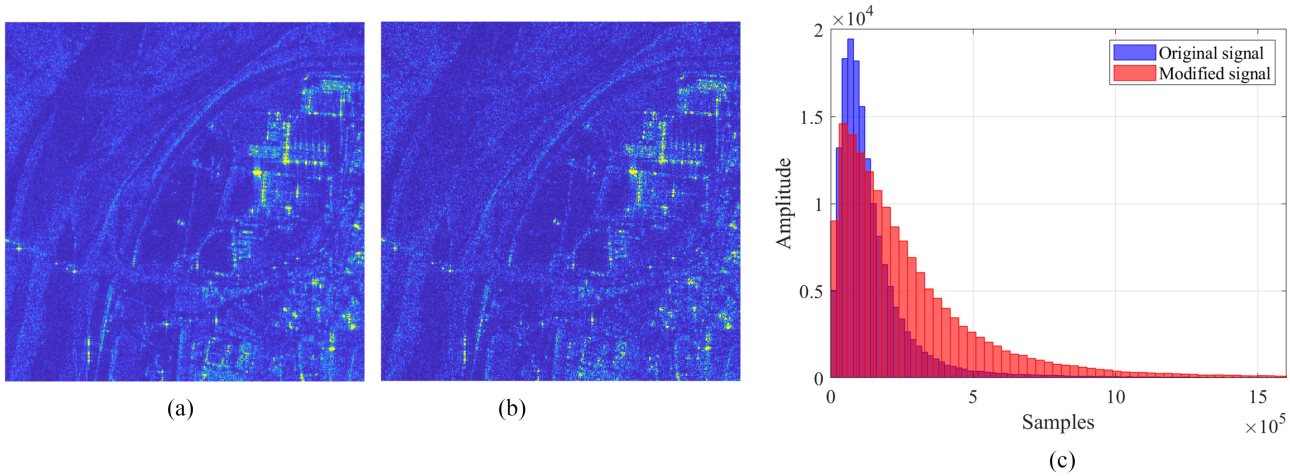

Fig. 3. Scene and probability histogram before and after inverse-whitening processing. (a) Scene before inverse-whitening processing. (b) Scene after inverse-whitening processing. (c) Probability histogram before and after inverse-whitening processing.

B. Construction of Sparse Transforming Domain

To achieve change imaging in the transforming domain, an appropriately sparse transforming dictionary is constructed in this section. First, the amplitude-based transforming dictionary $(\mathbf{D})^{abs}$ is constructed. Then, the transforming domains for the real and imaginary parts of the scene in the formula (6) are constructed based on $(\mathbf{D})^{abs}$ after the inverse-whitening processing.

Assuming that the amplitude-based vector-space of the transforming domain can be expressed as $(\mathbf{D})^{abs} = \{\boldsymbol{\xi}_1, \boldsymbol{\xi}_2, \ldots, \boldsymbol{\xi}_m, \ldots \boldsymbol{\xi}_M\}, \mathbf{D} \in \mathbb{R}^{M\times M}$. The constructed method of vector-space is given as follows. Take the historical observation $(\boldsymbol{\sigma}_0)^{abs}$ as one dimension of vector-space, i.e., $\boldsymbol{\xi}_m = (\boldsymbol{\sigma}_0)^{abs}$, and choose $m = 1$ without loss of generality. Each vector should be relatively orthogonal to ensure the reversibility of this transforming vector-space, i.e.,

$$\boldsymbol{\xi}_1^T \boldsymbol{\xi}_m = 0, m = 2, \ldots, M. \tag{10}$$

Therefore, the vector-space of the transforming domain is denoted as $(\mathbf{D})^{abs} = \{(\boldsymbol{\sigma}_0)^{abs}, orth(\mathbf{D}_{sub}, (\boldsymbol{\sigma}_0)^{abs})\}$, where $orth(\cdot)$ denotes the orthogonality operation, $(\mathbf{D}_{sub})^{abs} = \{\boldsymbol{\xi}_2, \ldots, \boldsymbol{\xi}_M\}$ is the $M \times (M-1)$ subspace. Assuming $\boldsymbol{\xi}_m = [\ \xi_{m,1} \quad \xi_{m,2} \quad \cdots \quad \xi_{m,M}\ ]^T$, The formula (10) is unfolded as

$$\begin{aligned} &|\sigma_1|\,\xi_{m,1} + |\sigma_2|\,\xi_{m,2} + \cdots + |\sigma_M|\,\xi_{m,M} \\ &\quad = 0, m = 2, 3, \ldots, M \end{aligned} \tag{11}$$

$\boldsymbol{\xi}_m$ has many solutions, the constructed method of which determines the sparse property of change. In this article, a simple constructed method of transforming vector-space is demonstrated, and it selects the pth dimension as the reference axis, i.e., $\xi_{m,p}$ is a constant. The formula (11) is written as

$$\begin{aligned} &|\sigma_1|\,\xi_{m,1} + \cdots + |\sigma_{p-1}|\,\xi_{m,p-1} + |\sigma_{p+1}|\,\xi_{m,p+1} \\ &\quad + \cdots |\sigma_M|\,\xi_{m,M} = -|\sigma_p|\,\xi_{m,p} \\ &m = 2, 3, \ldots, M \end{aligned} \tag{12}$$

so we have

$$\begin{aligned} \boldsymbol{\xi}_2 &= [-|\sigma_p|\,\xi_{2,p}/|\sigma_1|, 0, \ldots, 0, \xi_{2,p}, 0, \ldots, 0]^T \\ \boldsymbol{\xi}_3 &= [0, -|\sigma_p|\,\xi_{3,p}/|\sigma_2|, \ldots, 0, \xi_{3,p}, 0, \ldots, 0]^T \\ &\vdots \\ \boldsymbol{\xi}_M &= [0, 0, \ldots, 0, \xi_{M,p}, 0, \ldots, -|\sigma_p|\,\xi_{M,p}/|\sigma_M|]^T \end{aligned} \tag{13}$$

and then the transforming vector-space can be denoted as (14), shown at the bottom of the next page, where the constant dimension $\xi_{m,p}$ can be an arbitrary value, and it generally takes $\xi_{m,p} = 1$. Additionally, any dimension can be selected as the reference axis. To guarantee the stability of transforming vector-space, it usually takes the dimension of which the value in the historical observation $(\boldsymbol{\sigma}_0)^{abs}$ is the largest as the reference axis. The construction of the sparse transforming dictionary $(\mathbf{D})^{abs}$ based on the amplitude of historical observation is finished.

In this transforming domain, the sparse property of the change $(\Delta\boldsymbol{\sigma})^{abs}$ is explained by three following points.

1) *Similarity*: The current observation $(\boldsymbol{\sigma}_1)^{abs}$ is extremely similar to historical observation $(\boldsymbol{\sigma}_0)^{abs}$ so that the non-change part can be mapped on the dimension $\boldsymbol{\xi}_1$ constructed by historical observation $(\boldsymbol{\sigma}_0)^{abs}$, as illustrated in Fig. 4.
2) *Sparse property*: In the transforming domain, the sparse property of change $(\Delta\boldsymbol{\sigma})^{abs}$ depends on the subspace $(\mathbf{D}_{sub})^{abs}$ because most energy of the current observation is mapped on the dimension $\boldsymbol{\xi}_1$ of vector-space $(\mathbf{D})^{abs}$. When the subspace $(\mathbf{D}_{sub})^{abs}$ is a well-conditioned matrix, the change $(\Delta\boldsymbol{\sigma})^{abs}$ in the transforming domain is sparse. The well-conditioned property of transforming subspace is verified in the following. Assuming there are constants $\boldsymbol{\mathcal{A}}$ and $\boldsymbol{\mathcal{B}}$ for the nonzero vector $(\boldsymbol{\sigma})^{abs} \in \mathbb{R}^{M\times 1}$ so that [16]

$$\boldsymbol{\mathcal{A}} \le \frac{\left\|\left(\mathbf{D}_{sub}^T\right)^{abs}(\boldsymbol{\sigma})^{abs}\right\|_2^2}{\left\|(\boldsymbol{\sigma})^{abs}\right\|_2^2} \le \boldsymbol{\mathcal{B}} \tag{15}$$

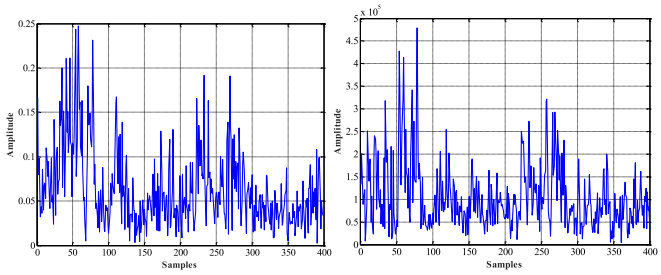

(a) (b)

Fig. 4. Historical observation $(\boldsymbol{\sigma}_0)^{abs}$ and the current observation $(\boldsymbol{\sigma}_1)^{abs}$. (a) Historical observation $(\boldsymbol{\sigma}_0)^{abs}$. (b) Current observation $(\boldsymbol{\sigma}_1)^{abs}$.

holds. We notice

$$\begin{aligned}&\frac{\left\|\left(\mathbf{D}_{sub}^{T}\right)^{abs}(\boldsymbol{\sigma})^{abs}\right\|_2^2}{\left\|(\boldsymbol{\sigma})^{abs}\right\|_2^2}\\&=\frac{\left[(\boldsymbol{\sigma})^{abs}\right]^{T}(\mathbf{D}_{sub})^{abs}\left(\mathbf{D}_{sub}^{T}\right)^{abs}(\boldsymbol{\sigma})^{abs}}{\left[(\boldsymbol{\sigma})^{abs}\right]^{T}(\boldsymbol{\sigma})^{abs}}\\&=\sum_{m=1}^{M}\delta_m\cos^2\theta_m\end{aligned}\tag{16}$$

where δ_m is the singular value of the matrix $(\mathbf{D}_{sub})^{abs}(\mathbf{D}_{sub}^{T})^{abs}$. θ_m is the angle between the mth singular vector of the matrix $(\mathbf{D}_{sub})^{abs}(\mathbf{D}_{sub}^{T})^{abs}$ and the vector $(\boldsymbol{\sigma})^{abs}$. Because different singular vectors are relatively orthogonal, we infer that A is the smallest singular value, i.e., $\delta_{\min}=\boldsymbol{\mathcal{A}}$, and $\boldsymbol{\mathcal{B}}$ is the largest singular value, i.e., $\delta_{\max}=\boldsymbol{\mathcal{B}}$. Therefore, the well-conditioned property of subspace can be explained by the singular value. Now the singular values of the matrix $(\mathbf{D}_{sub})^{abs}(\mathbf{D}_{sub}^{T})^{abs}$ are analyzed shown at the bottom of this page

Assuming $\xi_{m,p}=1$

$$\begin{aligned}&(\mathbf{D}_{sub})^{abs}\left(\mathbf{D}_{sub}^{T}\right)^{abs}\\&=|\sigma_p|^2\cdot diag\left(\begin{bmatrix}|\sigma_1|^{-2} & |\sigma_2|^{-2} & \cdots & |\sigma_{M-1}|^{-2}\end{bmatrix}\right)\\&\quad+\mathbf{1}^T\mathbf{1}\end{aligned}\tag{18}$$

where $\mathbf{1}$ denotes $\begin{bmatrix}1 & 1 & \cdots & 1\end{bmatrix}_{1\times(M-1)}^{T}$, $\mathbf{1}^T\mathbf{1}$ is the matrix where all the elements are equal to 1. $diag(\cdot)$ is the operation that converts the vector to the diagonal matrix. Since $|\sigma_p|\geq|\sigma_m|$, the inequality $|\sigma_p|^2/|\sigma_m|^2\geq 1$ holds. Assuming $\Omega=|\sigma_p|^2\cdot diag(\begin{bmatrix}|\sigma_1|^{-2} & |\sigma_2|^{-2} & \cdots & |\sigma_{M-1}|^{-2}\end{bmatrix})$, the matrix $(\mathbf{D}_{sub})^{abs}(\mathbf{D}_{sub}^{T})^{abs}$ can be regarded as adding the noise matrix $\mathbf{1}^T\mathbf{1}$ to the matrix Ω. Therefore, the singular value δ_m is approximately estimated by only considering Ω, so

$$\begin{aligned}\delta_{\max}\left((\mathbf{D}_{sub})^{abs}\left(\mathbf{D}_{sub}^{T}\right)^{abs}\right)&\approx\max\left(|\sigma_p/\sigma_m|^2\right)\\\delta_{\min}\left((\mathbf{D}_{sub})^{abs}\left(\mathbf{D}_{sub}^{T}\right)^{abs}\right)&\approx\min\left(|\sigma_p/\sigma_m|^2\right).\end{aligned}\tag{19}$$

According to the abovementioned formula (19), the singular value of the matrix $(\mathbf{D}_{sub})^{abs}(\mathbf{D}_{sub}^{T})^{abs}$ is decided by historical observation $(\boldsymbol{\sigma}_0)^{abs}$. The smallest singular value is

$$\delta_{\min}\approx\min\left(|\sigma_p/\sigma_m|^2\right)=|\sigma_p|^2\Big/\max\left(|\sigma_m|^2\right)=1\tag{20}$$

the largest singular value is

$$\delta_{\max}\approx\max\left(|\sigma_p/\sigma_m|^2\right)=|\sigma_p|^2\Big/\min\left(|\sigma_m|^2\right).\tag{21}$$

Assuming that $(\boldsymbol{\sigma}_0)^{abs}$ is the data after the quantification of u-mean and k times ς-standard variance, the condition number of the subspace $(\mathbf{D}_{sub})^{abs}$ is

$$cond\left((\mathbf{D}_{sub})^{abs}\right)\approx\frac{u+k\varsigma}{u-k\varsigma}\tag{22}$$

$$(\mathbf{D})^{abs}=\begin{bmatrix}|\sigma_1| & -|\sigma_p|\,\xi_{2,p}/|\sigma_1| & 0 & \cdots & 0\\|\sigma_2| & 0 & -|\sigma_p|\,\xi_{3,p}/|\sigma_2| & \cdots & 0\\\vdots & \vdots & \vdots & \ddots & \vdots\\|\sigma_{p-1}| & 0 & 0 & \cdots & 0\\|\sigma_p| & \xi_{2,p} & \xi_{3,p} & \cdots & \xi_{N,p}\\|\sigma_{p+1}| & 0 & 0 & \cdots & 0\\\vdots & \vdots & \vdots & \ddots & \vdots\\|\sigma_M| & 0 & 0 & \cdots & -|\sigma_p|\,\xi_{N,p}/|\sigma_N|\end{bmatrix}\tag{14}$$

$$(\mathbf{D}_{sub})^{abs}\left(\mathbf{D}_{sub}^{T}\right)^{abs}=\begin{bmatrix}\left(|\sigma_p|\,\xi_{2,p}/|\sigma_1|\right)^2+\xi_{2,p}^2 & \xi_{2,p}\xi_{3,p} & \cdots & \xi_{2,p}\xi_{M,p}\\\xi_{3,p}\xi_{2,p} & \left(|\sigma_p|\,\xi_{3,p}/|\sigma_2|\right)^2+\xi_{3,p}^2 & \cdots & \xi_{3,p}\xi_{M,p}\\\vdots & \vdots & \ddots & \vdots\\\xi_{M,p}\xi_{2,p} & \xi_{M,p}\xi_{3,p} & \cdots & \left(|\sigma_p|\,\xi_{M,p}/|\sigma_{M-1}|\right)^2+\xi_{M,p}^2\end{bmatrix}.\tag{17}$$

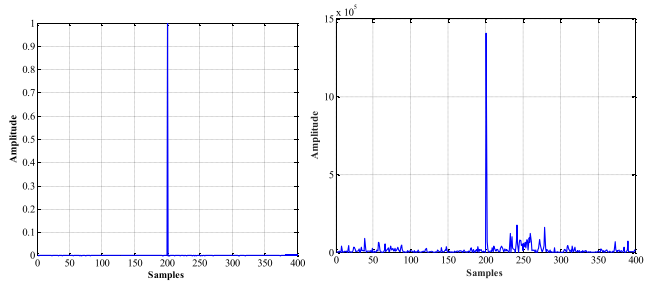

Fig. 5. Historical observation $(\boldsymbol{\sigma}_0)^{abs}$ and the current observation $(\boldsymbol{\sigma}_1)^{abs}$ in the amplitude-based transforming domain. (a) $(\boldsymbol{\sigma}_0)^{abs}$ in the amplitude-based transforming domain. (b) $(\boldsymbol{\sigma}_1)^{abs}$ in the amplitude-based transforming domain.

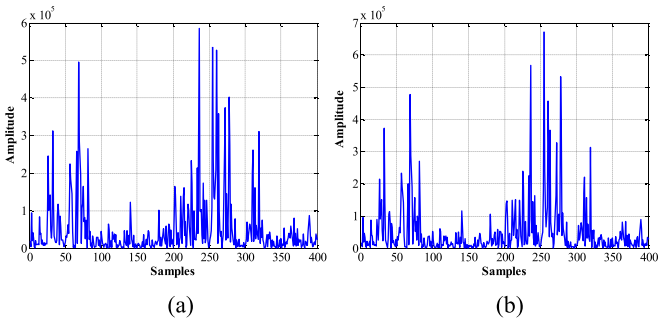

Fig. 6. After the inverse-whitening, $\boldsymbol{\sigma}_{\text{new}}^{real}$ and $\boldsymbol{\sigma}_{\text{new}}^{imag}$ in the amplitude-based transforming domain. (a) $\boldsymbol{\sigma}_{\text{new}}^{\text{real}}$ in the amplitude-based transforming domain. (b) $\boldsymbol{\sigma}_{\text{new}}^{imag}$ in the amplitude-based transforming domain.

where $cond(\cdot)$ denotes the condition number, u and ς is the mean and standard variance of the historical observation $(\boldsymbol{\sigma}_0)^{abs}$. As we all know, the closer to 1 the condition number of the matrix is, the better the well-conditioned property of the matrix is. Generally, the dynamic range of SAR image is not large. When the quantitative number k is not large [14], the condition number is not large so that the subspace $(\mathbf{D}_{sub})^{abs}$ has the well-conditioned property. Therefore, the sparse property of change $(\Delta\boldsymbol{\sigma})^{abs}$ is guaranteed by the well-conditioned subspace $(\mathbf{D}_{sub})^{abs}$and is demonstrated in Fig. 5 by the signal in Fig. 4 mapped on the transforming dictionary $(\mathbf{D})^{abs}$, where the change $(\Delta\boldsymbol{\sigma})^{abs}$is circularly shifted for the sake of presentation.

3) *Ignoring the speckle noise*: Since the transforming dictionary $(\mathbf{D})^{abs}$ has changed little about the signal amplitude, and the speckle noise is generally small, it can be ignored in the sparse reconstruction.

After the construction of the amplitude-based transforming dictionary $(\mathbf{D})^{abs}$, the following is the construction of the sparse transforming domain for the real and imaginary parts of the scene based on $(\mathbf{D})^{abs}$. Because the signs of real and imaginary parts are not consistent with that of the amplitude part, the real and imaginary parts of the scene after inverse-whitening processing are not sparse in the sparse transforming domain $(\mathbf{D})^{abs}$, as illustrated in Fig. 6.

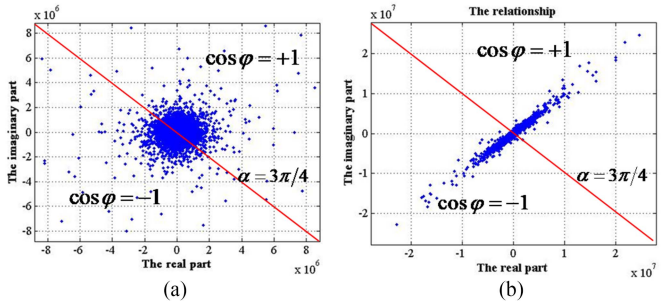

Fig. 7. Sign segmentation of the scene before and after inverse-whitening processing. (a) Sign segmentation before inverse-whitening processing. (b) Sign segmentation after inverse-whitening processing.

The real and imaginary parts are represented by

$$\boldsymbol{\sigma}_{\text{new}}^{\text{real}} = \text{sgn}\left(\boldsymbol{\sigma}_{\text{new}}^{\text{real}}\right) \cdot \left|\boldsymbol{\sigma}_{\text{new}}^{\text{real}}\right|, \boldsymbol{\sigma}_{\text{new}}^{imag} = \text{sgn}\left(\boldsymbol{\sigma}_{\text{new}}^{imag}\right) \cdot \left|\boldsymbol{\sigma}_{\text{new}}^{imag}\right|. \tag{23}$$

The inverse-whitening processing does not change signs of variables, so (23) can be further simplified as

$$\boldsymbol{\sigma}_{\text{new}}^{\text{real}} = \text{sgn}\left(\boldsymbol{\sigma}^{\text{real}}\right) \cdot \left|\boldsymbol{\sigma}_{\text{new}}^{\text{real}}\right|, \boldsymbol{\sigma}_{\text{new}}^{imag} = \text{sgn}\left(\boldsymbol{\sigma}^{imag}\right) \cdot \left|\boldsymbol{\sigma}_{\text{new}}^{imag}\right|. \tag{24}$$

The sign should be first determined to ensure change imaging in the transforming domain $\mathbf{D}$. The best segmentation line of Figs. 1(a) and 2(a) is $\alpha = 3\pi/4$, as illustrated in Fig. 7, where α and φ are the segmentation angle and the scene phase.

Then, the sign of the real part is

$$\text{sgn}\left(\boldsymbol{\sigma}^{\text{real}}\right) = \begin{cases} 1, -\frac{\pi}{4} \le \text{angle}\left(\boldsymbol{\sigma}\right) < \frac{3\pi}{4} \\ -1, others \end{cases}. \tag{25}$$

Notice that

$$\text{sgn}\left(\boldsymbol{\sigma}^{\text{real}}\right) + \text{sgn}\left(\boldsymbol{\sigma}^{imag}\right) = 0 \tag{26}$$

so

$$\text{sgn}\left(\boldsymbol{\sigma}^{imag}\right) = \begin{cases} -1, -\frac{\pi}{4} \le \text{angle}\left(\boldsymbol{\sigma}\right) < \frac{3\pi}{4} \\ 1, others \end{cases}. \tag{27}$$

The transforming dictionaries of the real and imaginary parts are denoted as

$$\begin{aligned} \mathbf{D}_{\text{new}}^{\text{real}} &= (\mathbf{D})^{abs} \cdot diag\left\{\text{sgn}\left(\boldsymbol{\sigma}^{\text{real}}\right)\right\} \\ \mathbf{D}_{\text{new}}^{imag} &= (\mathbf{D})^{abs} \cdot diag\left\{\text{sgn}\left(\boldsymbol{\sigma}^{imag}\right)\right\}. \end{aligned} \tag{28}$$

C. Change Imaging in the Transforming Domain

Based on the inverse-whitening processing, the observation model (6) is

$$\begin{aligned} &\begin{bmatrix} \mathbf{y}^{\text{real}} \\ \mathbf{y}^{imag} \end{bmatrix} \\ &= \begin{bmatrix} p_{11}\mathbf{A}^{\text{real}} - p_{21}\mathbf{A}^{imag} & p_{12}\mathbf{A}^{\text{real}} - p_{22}\mathbf{A}^{imag} \\ p_{11}\mathbf{A}^{imag} + p_{21}\mathbf{A}^{\text{real}} & p_{12}\mathbf{A}^{imag} + p_{22}\mathbf{A}^{\text{real}} \end{bmatrix} \\ &\quad \begin{bmatrix} \mathbf{D}_{\text{new}}^{\text{real}} \cdot \Delta\boldsymbol{\sigma}_{\text{new}}^{\text{real}} \\ \mathbf{D}_{\text{new}}^{imag} \cdot \Delta\boldsymbol{\sigma}_{\text{new}}^{imag} \end{bmatrix} + \begin{bmatrix} \mathbf{n}^{\text{real}} \\ \mathbf{n}^{imag} \end{bmatrix}. \end{aligned} \tag{29}$$

The change $\Delta\boldsymbol{\sigma}_{\text{new}}^{\text{real}}$ and $\Delta\boldsymbol{\sigma}_{\text{new}}^{imag}$ are sparse in the transforming domain $\mathbf{D}_{\text{new}}^{\text{real}}$ and $\mathbf{D}_{\text{new}}^{imag}$, respectively. And it can be illustrated

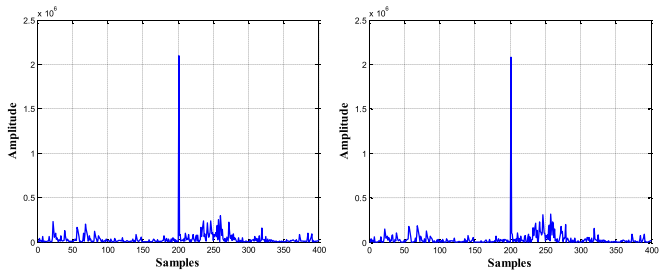

Fig. 8. Change $\Delta\boldsymbol{\sigma}_{\text{new}}^{\text{real}}$ and $\Delta\boldsymbol{\sigma}_{\text{new}}^{imag}$ in the transforming domain $\mathbf{D}_{\text{new}}^{\text{real}}$ and $\mathbf{D}_{\text{new}}^{imag}$, respectively. (a) Change $\Delta\boldsymbol{\sigma}_{\text{new}}^{\text{real}}$ in the transforming domain $\mathbf{D}_{\text{new}}^{\text{real}}$. (b) Change $\Delta\boldsymbol{\sigma}_{\text{new}}^{imag}$ in the transforming domain $\mathbf{D}_{\text{new}}^{imag}$.

Algorithm: Reconstruction Based on the Real-Imaginary Separated Operation.

Initialization: $(\boldsymbol{\sigma}_0)^{abs}$, $\mathbf{A}$, $\mathbf{y}$, $\mathbf{P}$;

1. Construct the transform dictionary $(\mathbf{D})^{abs}$ by (14);
2. Calculate the initial result $\boldsymbol{\sigma}_{MF}$ based on matched filter;
3. Acquire the sign $\text{sgn}(\boldsymbol{\sigma}^{real})$ and $\text{sgn}(\boldsymbol{\sigma}^{imag})$ based on $\boldsymbol{\sigma}_{MF}$;
4. Calculate the transforming dictionary $\mathbf{D}_{new}^{real}$ and $\mathbf{D}_{new}^{imag}$;
5. Solve the optimization (29) by CS algorithms [17], [18], [19];
6. Acquire the final image by (30).

in Fig. 8. We adopt the CS algorithms [17], [18], [19] to recover the change $\left[\ \Delta\boldsymbol{\sigma}_{\text{new}}^{\text{real}} \quad \Delta\boldsymbol{\sigma}_{\text{new}}^{imag}\ \right]^T$ by solving (29).

After the recovery of change, a real SAR image can be acquired by

$$\begin{bmatrix} \left(\boldsymbol{\sigma}^{\text{real}}\right)^T \\ \left(\boldsymbol{\sigma}^{imag}\right)^T \end{bmatrix} = \mathbf{P} \cdot \begin{bmatrix} \left(\mathbf{D}_{\text{new}}^{\text{real}} \Delta\boldsymbol{\sigma}_{\text{new}}^{\text{real}}\right)^T \\ \left(\mathbf{D}_{\text{new}}^{imag} \Delta\boldsymbol{\sigma}_{\text{new}}^{imag}\right)^T \end{bmatrix}. \tag{30}$$

At last, the terminated condition can be determined by the loss function

$$\left| L\left(\boldsymbol{\sigma}^{k+1}\right) - L\left(\boldsymbol{\sigma}^{k}\right) \right| < \iota \tag{31}$$

where $L(\boldsymbol{\sigma}) = \|\mathbf{y} - \mathbf{A}\sigma\|_2^2$, and ι is the error threshold, which usually takes 10^{-3} [20]. The procedure of change imaging in the transforming domain is presented as follows.

IV. Experimental Results

The recovered performance based on CS depends on sparsity, signal-noise ratio (SNR), and the undersampling ratio. In this article, we analyze the sparse property of change in the transforming domain in a numerical test environment first. Then, the proposed change imaging in the transforming domain is verified in terms of the recovered performance under different SNRs. Experiments on simulated and real SAR images both verify the effectiveness of our proposed algorithm.

TABLE I
Simulated Parameters

Parameter	Value
Range sampling frequency (MHz)	118.6
Referred slant range (km)	784.16
Chirp rate (Hz/s)	10^{12}
Pulse width (us)	8
Wavelength (m)	0.24
Velocity (m/s)	7550
Height (km)	633

In our experiments, two scenes, which include two optical images and four SAR images were used in the experimental part of this article, and preprocessing, such as alignment and correction, was performed before the experiments. Fig. 9 shows the first experimental data observed in a city located in Yamanashi Prefecture in Japan, where Fig. 9(a) is the optical images achieved by Google Earth on 2014/6/15, while Fig. 9(b) and (c) are 3 m SAR images achieved by ALOS-2 satellite radar on 2014/10/28 and 2014/11/11, respectively. Fig. 10 shows the second experimental data observed on some buildings around Xueyuan Road in Beijing, China, where Fig. 10(a) is the optical images observed on Google Earth on 2020/8/28, while Fig. 10(b) and (c) are 1 m SAR images achieved by TerraSAR-X satellite radar on 2020/10/16 and 2020/10/27, respectively. Two types of changes are labeled in the scene Fig. 10(b) and (c). One is the increased parts circled by red lines. It means these targets do not exist in Fig. 10(b) but exist in Fig. 10(c). The other is the decreased parts circled by yellow lines. It means these targets exist in Fig. 10(b) but do not exist in Fig. 10(c).

Temporal and spatial consistencies are represented by time interval and incidence angle difference, respectively. In (b) and (c) of Figs. 9 and 10, the time intervals are 14 days and 11 days, and the incidence angle differences are 0.5320 ° and 0.0092 °, respectively. Therefore, it can be confirmed that current observation (c) has temporal and spatial consistencies with historical observation (b) so that it can ensure the sparse property of change $(\Delta\boldsymbol{\sigma})^{abs}$ required by CS reconstruction. SAR echoes are generated according to the parameters in Table I and the scene in Figs. 9 and 10. For a given under-recovered signal $\boldsymbol{\sigma}$, the recovered performance can be evaluated by mean square error (MSE)

$$\text{MSE} = \|\hat{\sigma} - \boldsymbol{\sigma}\|_2^2 \tag{32}$$

where $\hat{\sigma}$ is the recovered scene.

A. Sparse Property of the Transforming Domain

Sparse property is the requirement of change imaging in the transforming domain based on CS algorithms. The Wavelet dictionary [21], [22] and the identity matrix $\mathbf{I}$ are introduced to compare the sparse property with that of the proposed sparse transforming domain in Section III. An identity matrix $\mathbf{I}$ is

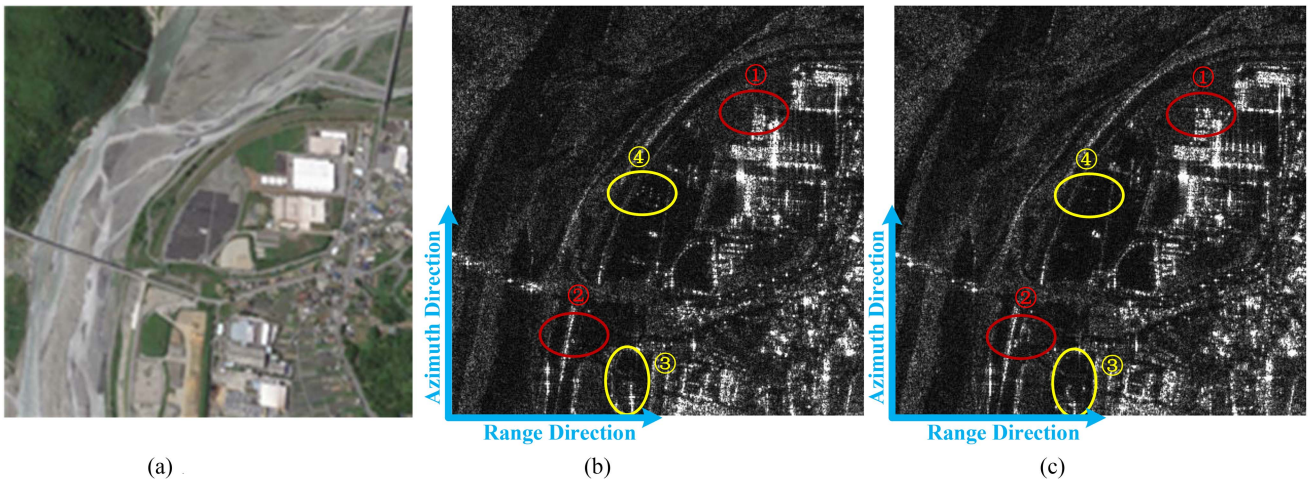

Fig. 9. Optical image, historical SAR image, and current SAR image observed in a city located in Yamanashi Prefecture in Japan. (a) Optical image. (b) Historical SAR image. (c) Current SAR image.

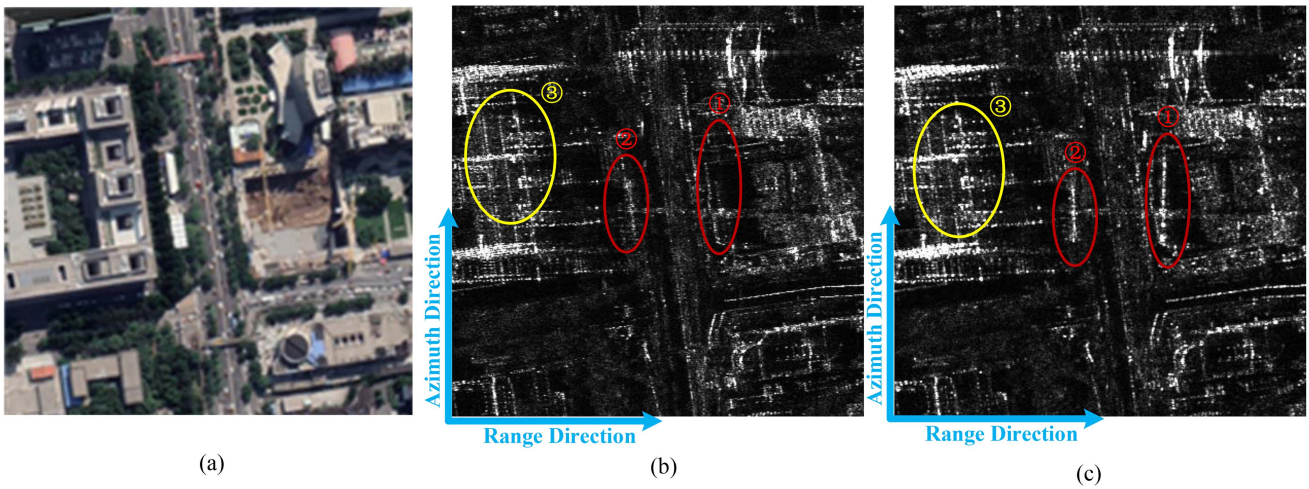

Fig. 10. Optical image, historical SAR image, and current SAR image observed in the Buildings around Xueyuan Road, Beijing, China. (a) Optical image. (b) Historical SAR image. (c) Current SAR image.

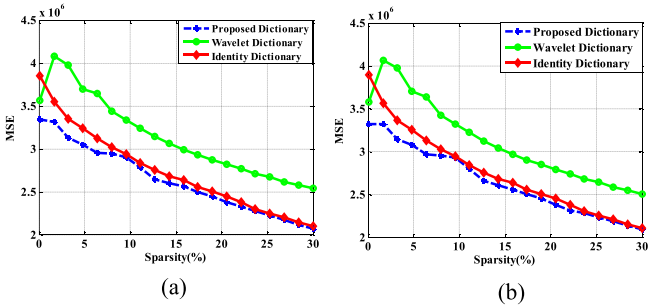

Fig. 11. Recovered performance against sparsity of change's real and imaginary parts. The blue and green lines are the results based on the Wavelet dictionary and our proposed transforming domain, respectively. The red line is the result after the processing under different sparse thresholds. (a) Recovered performance against sparsity of change's real part. (b) Recovered performance against sparsity of change's imaginary part.

an ideal dictionary. At the same sparsity level of change, the more accurate the representation in the transforming domain, the better the performance of the transforming dictionary, and the sparser the change. The procedure of simulation is demonstrated, First, the change $(\Delta\boldsymbol{\sigma})^{abs}$ is achieved by comparing Fig. 8(b) and (c), and then we set different threshold values z to change the sparsity of change. The values of change that are smaller than the threshold value are set to zero, and the rest remains. This change is denoted as $(\Delta\boldsymbol{\sigma})_z^{abs}$. Considering the wavelet dictionary and our proposed transforming domain, the current observation is $\boldsymbol{\sigma}_z = \mathbf{D}(\Delta\boldsymbol{\sigma})_z^{abs}$. As for the identity dictionary, the current observation is $\boldsymbol{\sigma}_z = \boldsymbol{\sigma}_0 + (\Delta\boldsymbol{\sigma})_z^{abs}$. The performance of the transforming domain is evaluated by $\|\boldsymbol{\sigma} - \boldsymbol{\sigma}_z\|_2^2$. In this section, two scenes of Figs. 9 and 10 are selected to verify the sparse property of the proposed transforming domain.

The simulation in Fig. 11 demonstrates that the proposed transforming domain $\mathbf{D}$ after inverse-whitening processing can achieve the approximated result with the identity matrix. Occasionally, the proposed transforming domain performs better. This is because the inverse-whitening processing concentrates most components of current observation on the historical

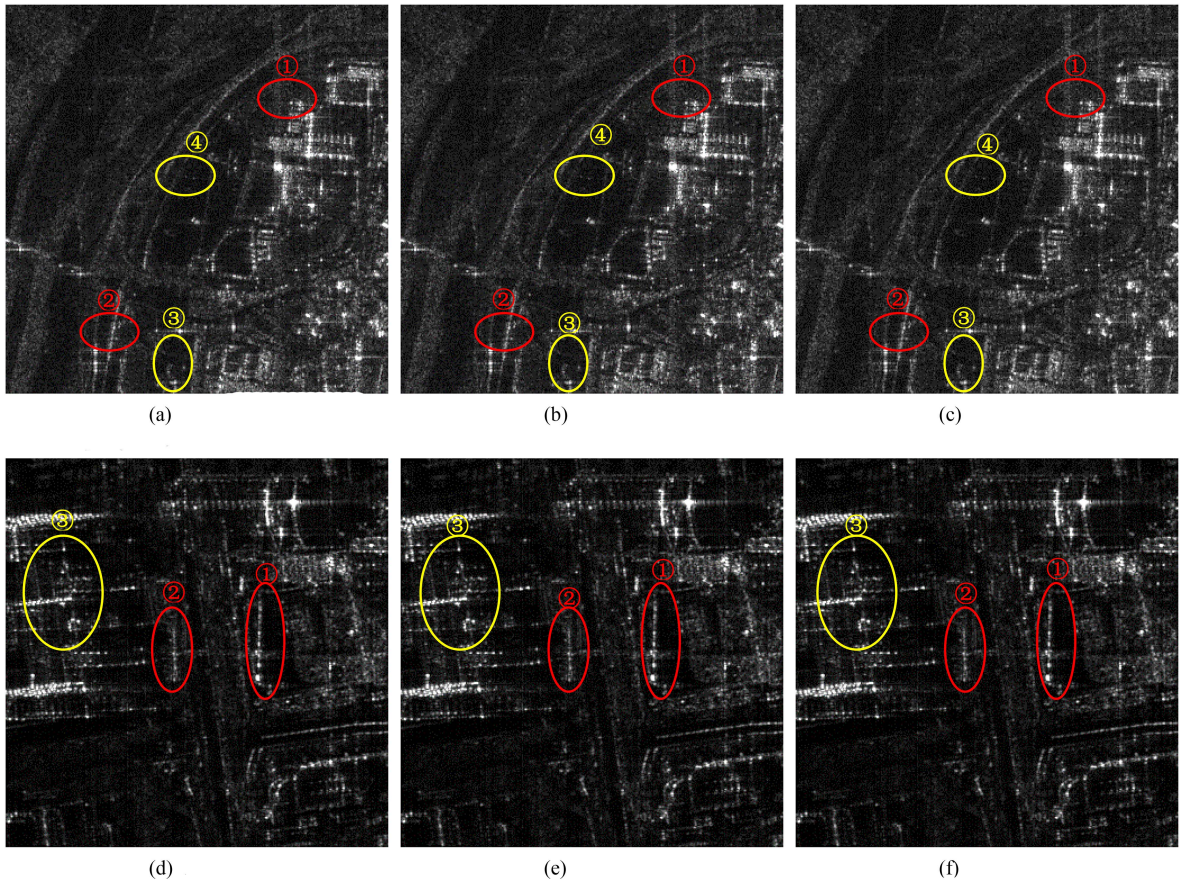

Fig. 12. Results of change imaging in the transforming domain with the 10-, 20-, and 30-times undersampling ratio while no noise exists. (a) Recovered result with the 10-times undersampling echo. (b) Recovered result with the 20-times undersampling echo. (c) Recovered result with the 30-times undersampling echo. (d) Recovered result with the 10-times undersampling echo. (e) Recovered result with the 20-times undersampling echo. (f) Recovered result with the 30-times undersampling echo.

observation so that the change is sparser. In a short, the proposed transforming domain ensures the sparse property required by CS algorithms.

B. Recovered Performance Against Undersampling Ratio Under Different SNR

In this section, we simulate the reconstructed performance against the undersampling ratio under different SNRs. SNR refers to that of the raw data after the range signal is compressed. The recovered results are achieved with echoes under different undersampling ratios by our proposed change imaging in the transforming domain based on CS. The simulated results in Fig. 12 and the performance curves in Fig. 13 demonstrate the effectiveness of our proposed algorithm. In Fig. 12, the proposed algorithm can recover the scene very well with echoes under the 10-, 20-, and 30-times undersampling ratio without noise. The details of the increased part in red circles or decreased part in yellow circles are perfectly focused and recognized. In Fig. 13, we simulate the curves of recovered performance against the undersampling ratio under different SNRs. Low SNR affects the recovered results. Fortunately, SNR is larger than 0 dB after the range is compressed for most SAR systems. Therefore, the recovered results are better under the SNR larger than 0 dB.

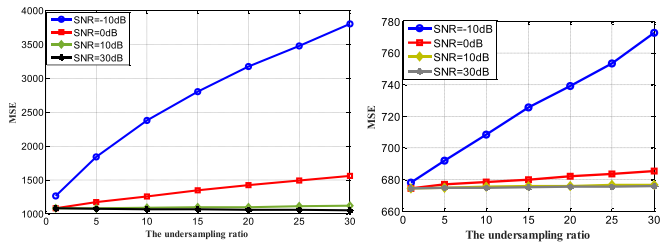

Fig. 13. Performance curve of change imaging in the transforming domain against different undersampling ratios. (a) Performance curve of change imaging in the transforming domain against different undersampling ratios in the first scene. (b) Performance curve of change imaging in the transforming domain against different undersampling ratios in the second scene.

C. Simulation Results Comparison of Increment Imaging in the Spatial Domain and Change Imaging in the Transform Domain

Increment imaging [13] requires that the current observation has the same quantification level with the historical observation. To further reflect the performance of our proposed algorithm, we also quantized the recovery results $(\hat{\sigma}_1)^{abs}$ at the same level as [13], i.e., $(\hat{\sigma}_1)^{abs\_q}$, where the newly added superscript q

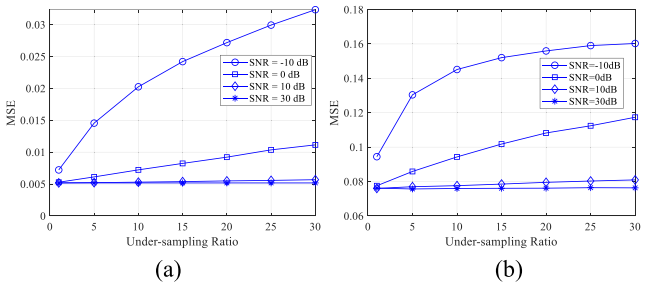

Fig. 14. Performance curves against under-sampling ratio in different SNRs. (a) Performance curve of increment imaging against different undersampling ratios in the first scene. (b) Performance curve of change imaging in the transforming domain against different undersampling ratios in the first scene.

represents quantification. The performance curves are shown in Fig. 14, and it can be seen that the reconstruction error is almost 10-times of [13]. However, this does not mean that the algorithm is meaningless, and the proposed method offers an alternative in change imaging but does not necessarily improve reconstructed performance over [13].

The changes $(\Delta\boldsymbol{\sigma})^{abs\_q}$ of increment imaging in [13] exist in the spatial domain, i.e., $(\boldsymbol{\sigma}_1)^{abs\_q} = (\boldsymbol{\sigma}_0)^{abs\_q} + (\Delta\boldsymbol{\sigma})^{abs\_q}$, where the newly added superscript q represents quantification. To make compare, these two SAR images should be quantified at the same level. Therefore, the algorithm proposed in [13] should own the ability to estimate the quantification accurately. That is why the uniform quantification matrix is introduced in [13]. To make the algorithm general, the historical image data $(\boldsymbol{\sigma}_0)^{abs\_q}$ is quantified into 0∼1. Therefore, the MSE of estimated spatial changes $(\Delta\boldsymbol{\sigma})^{abs\_q}$ will be very small, i.e., the order of magnitude in Fig. 14(a). However, the changes in this proposed algorithm lie in the transform domain. It avoids estimating the quantification level directly, making it more applicable. The sparsity depends on the transform dictionary $\mathbf{D}$. That means the recovery errors not only have the part of changes but also mixed with some parts introduced by $\mathbf{D}$. Therefore, compared with errors introduced only by $(\Delta\boldsymbol{\sigma})^{abs\_q}$ in [13], the recovery error in the transform domain is essentially larger.

To implement the sparse changes in [13], it is necessary to ensure that the position in each resolution grid is sufficiently accurate, and the quantification level should be estimated accurately as well. That means the historical image data should be of high quality, acting as a strong prior. However, the proposed algorithm is based on a transform domain dictionary constructed by using the structural features of historical data. It focuses on the similarity between historical data and current observations and has very low requirements for specific values. It means a weak prior. The reduced constraints lead to an increase in estimation error, which is worthwhile for the generality of observation. From the simulation results, although the overall accuracy has degenerated, the effective imaging of the changing targets can still be guaranteed, as shown in Fig. 12.

V. Conclusion

In this article, we propose SAR change imaging in the transforming domain, which converts the recovery of the scene itself to the recovery of the change, to increase the universality and availability of CS-SAR imaging. First, the complex-valued sparse problem is solved by the real-imaginary separated operation. Then, inverse-whitening processing is introduced and the sparse transform domain is constructed based on this processing and the prior amplitude of historical observation to ensure the sparse property of the real and imaginary parts of change. Finally, CS algorithms recover the change to achieve change imaging in the transforming domain. Experiments carried out on simulated and real-measured SAR images demonstrate the effectiveness and the advanced accuracy of the proposed method by the curves of recovered performance.

Based on this imaging processing method, the undersampling raw data can be recovered well so that the contradiction between high resolution and wide swath can be further relieved. Therefore, the potential applications of this proposed method may achieve an HRWS system. Note that the proposed method converts complex-data operations to matrix operations, this will take up a large amount of memory resources to achieve large scene recovery. A multichannel processing scheme may have great potential for this article and deserves further attention.

References

[1] I. G. Cumming and F. H. Wong, *Digital Processing of Synthetic Aperture Radar Data: Algorithms and Implementation*. Norwood, MA, USA: Artech House, 2004.
[2] E. J. Candes and T. Tao, "Decoding by linear programming," *IEEE Trans. Inf. Theory*, vol. 51, no. 12, pp. 4203–4215, Dec. 2005.
[3] D. L. Donoho, M. Elad, and V. N. Temlyakov, "Stable recovery of sparse overcomplete representations in the presence of noise," *IEEE Trans. Inf. Theory*, vol. 52, no. 1, pp. 6–18, Jan. 2006.
[4] R. G. Baraniuk, "Compressive sensing," *IEEE Signal Process. Mag.*, vol. 24, no. 4, pp. 118–121, Jul. 2007.
[5] Z. Yu, W. Chen, P. Xiao, and C. Li, "AgileSAR: Achieving wide-swath spaceborne SAR based on time-space sampling," *IEEE Access*, vol. 7, pp. 674–686, 2019.
[6] W. Chen, C. Li, Z. Yu, and P. Xiao, "Sub-Nyquist SAR based on pseudo-random time-space modulation," *Sensors*, vol. 18, pp. 4343–4343, 2018.
[7] G. D. Martino and A. Iodice, "Coprime synthetic aperture radar (CopSAR): A new acquisition mode for maritime surveillance," *IEEE Trans. Geosci. Remote Sens.*, vol. 53, no. 6, pp. 3110–3123, Jun. 2015.
[8] P. Snoeij et al., "Sentinel-1 radar mission: Status and performance," *IEEE Aerosp. Electron. Syst. Mag.*, vol. 25, no. 8, pp. 32–39, Aug. 2010.
[9] I. Sikaneta, C. H. Gierull, and D. Cerutti-Maori, "Optimum signal processing for multichannel SAR: With application to high-resolution wideswath imaging," *IEEE Trans. Geosci. Remote Sens.*, vol. 52, no. 10, pp. 6095–6109, Oct. 2014.
[10] G. Krieger, "MIMO-SAR: Opportunities and pitfalls," *IEEE Trans. Geosci. Remote Sens.*, vol. 52, no. 5, pp. 2628–2645, May 2014.
[11] J. C. Curlander and R. N. McDonough, *Synthetic Aperture Radar: Systems and Signal Processing*. New York, NY, USA: Wiley, 1991.
[12] H. Bi, C. Jiang, B. Zhang, Z. Wang, and W. Hong, "Radar change imaging with undersampled data based on matrix completion and Bayesian compressive sensing," *IEEE Geosci. Remote Sens. Lett.*, vol. 12, no. 7, pp. 1546–1550, Jul. 2015.
[13] J. Geng, Z. Yu, and C. Li, "Synthetic aperture radar increment imaging based on compressed sensing," *IEEE Geosci. Remote Sens. Lett.*, vol. 19, 2022, Art. no. 4013705.
[14] C. Oliver and S. Quegan, *Understanding Synthetic Aperture Radar Images*. Norwood, MA, USA: Artech House, 1998.
[15] S. M. Kay, *Fundamentals of Statistical Signal Processing*. New York, NY, USA: Prentice-Hall, 1998.
[16] J. L. Starck, F. Murtagh, and J. Fadili, *Sparse Image and Signal Processing: Wavelets and Related Geometric Multiscale Analysis*. Cambridge, U.K.: Cambridge Univ. Press, 2015.

[17] C. Soussen, R. Gribonval, J. ldier, and C. Herzet, "Joint K-Step analysis of orthogonal matching pursuit and orthogonal least squares," *IEEE Trans. Inf. Theory*, vol. 59, no. 5, pp. 3158–3174, May 2013.
[18] E. Candes and T. Tao, "The dantzig selector: Statistical estimation when p is much larger than n," *Ann. Statist.*, vol. 35, pp. 2313–2351, 2007.
[19] S. Ji, Y. Xue, and L. Carin, "Bayesian compressive sensing," *IEEE Trans. Signal Process.*, vol. 56, no. 6, pp. 2346–2356, Jun. 2008.
[20] H. Liu, J. Hu, Y. Li, and Z. Wen, "Constrained optimization," in *Optimization: Modeling, Algorithms and Theory*, 1st ed. Beijing, China: Higher Education Press, 2020, pp. 311–330.
[21] N. Vaswani, "Kalman filtered compressed sensing," in *Proc. 15th IEEE Int. Conf. Image Process.*, 2008, pp. 893–896.
[22] M. Lustig, D. Donoho, and J. M. Pauly, "Sparse MRI: The application of compressed sensing for rapid MR imaging," *Magn. Reson. Med.*, vol. 58, no. 6, pp. 1182–1195, 2014.

Wenjiao Chen received the Ph.D. degree in communication and information systems from Beihang University, Beijing, China, in 2020.

She is currently a Lecture with Space Engineering University, Beijing, China. Her research interests include system design and signal processing for a wide-swath synthetic aperture radar, as well as system performance analysis for an aperture radar.

Jiwen Geng was born in Nanjing, China, in 1990. He received the B.S. degree in information engineering from Yangzhou University, Yangzhou, China, in 2013, and the Ph.D. degree in signal and information processing from the School of Electronics and Information Engineering, Beihang University, Beijing, China, in 2021.

He is currently a Postdoctoral Fellow with Southeast University, Nanjing, China. His research interests include SAR imaging algorithm design, compressed sensing, sparsity representation, and Bayesian Inference.

Ze Yu (Member, IEEE) was born in Xi'an, China, in 1979. He received the B.S. degree in electronics engineering and the Ph.D. degree in communication and information system from Beihang University, Beijing, China, in 2002 and 2007, respectively.

Since 2009, he has been with the School of Electronics and Information Engineering, Beihang University. He is currently involved in the system design and imaging processing for high-resolution and wideswath synthetic aperture radar.

Yukun Guo was born in Beijing, China, in 1990. He received the B.S. degree in electronics engineering in 2013 from Beihang University, Beijing, China, where he is currently working toward the Ph.D. degree in signal and information processing.

His research interests include system performance analysis and signal processing for multistatic synthetic aperture radar.